



LCC-S compensated variable inductor-based hybrid topology analysis for inductive power transfer system

Ekrem Kandemir¹ · Selim Borekci²

Received: 25 April 2023 / Accepted: 24 August 2023 / Published online: 23 September 2023
© The Author(s), under exclusive licence to Springer-Verlag GmbH Germany, part of Springer Nature 2023

Abstract

Inductive power transfer (IPT) technology is widely used in the automobile industry, household electronics, and medical devices because of its numerous advantages. This manuscript proposes a novel hybrid topology for inductive power transfer (IPT) systems, combining the series–series (SS) and inductance–capacitance–capacitance–series (LCC-S) circuitries. The study introduces several key novelties to improve battery charging efficiency and reliability. Firstly, the hybrid topology achieves a load-independent zero phase angle (ZPA) condition at a constant resonant frequency, eliminating the need for frequency variation between constant current (CC) and constant voltage (CV) charging modes by introducing a tunable inductor and an AC switch. That results in simplified control circuit. In addition, it eliminates the need for variable resonant frequency control or coupling coefficient tuning to achieve CC and CV charging operations at a constant resonant frequency. Moreover, the proposed topology extends circuit lifespan and reliability by minimizing the number of capacitors required. Simulation analysis of a 2.4 kW prototype charging system was implemented in PLECS with MATLAB/Simulink to confirm the feasibility and operating performance of the proposed design. According to the results, the proposed topology successfully realizes stable CC and CV charging with ZPA condition at 85 kHz single resonant frequency even under different load conditions. The maximum power of 2.4 kW was achieved with 98.66% efficiency for an equivalent battery load of 67 Ω and a coupling factor of 0.3585. Additionally, a comparison review of CC/CV charging capability, control complexity, and cost-effectiveness between existing circuits and the designed topology are presented in the discussion of this paper.

Keywords Inductive power transfer · Switching hybrid topology · Series–series compensation · Inductance–capacitance–capacitance–series compensation · Electric vehicle

1 Introduction

Inductive power transfer (IPT) devices have attracted great interest with their inherent advantages such as electrical isolation, safety and reliability [1, 2]. Additionally, IPT is less time-consuming, causes less pollution and is safe to use in a wet environment than the plug-in charging system, which has disadvantages of safety and reliability issues such as electric sparks, contact losses and mechanical corrosion [3]. However, IPT devices provide less efficiency than plug-in charging systems due to the low coupling coefficient [4, 5]. Despite these situations mentioned above, IPT systems

have been widely preferred to make efficient battery charging in fields such as mobile phones, wireless charging medical apparatus, and electric vehicles (EV) [3, 6, 7].

In the discussed applications above, the lithium-ion (Li-ion) battery has been generally preferred due to their reliability, high-performance, high-power density and longevity [6, 8]. However, constant current (CC) and constant voltage (CV) charging modes are required for efficient charging and prolonging the lifetime of Li-ion batteries [9]. Generally, the battery charging starts with the CC charging process and moves to the CV process when the battery voltage reaches a defined value [6]. At CC charging mode, the battery voltage rises depending on the battery characteristics, but the battery current remains the same. On the other hand, at CV charging mode, the battery current starts to decrease depending on the battery requirement, but the charging voltage remains the same. Eventually, the charging is terminated when the battery current decreases to a specific level.

✉ Ekrem Kandemir
ekrem.kandemir@tubitak.gov.tr

¹ TUBITAK National Observatory, Antalya, Turkey

² Department of Electrical & Electronics Engineering, Akdeniz University, Antalya, Turkey

Since the Li-ion battery is expensive, an efficient charging strategy is necessary to decrease charging time, optimal charging modes and energy efficiency for battery health [4]. To achieve desired CC and CV charging profiles in IPT systems, various conventional circuitries have been studied to perform CC/CV charging, such as variable frequency control, special tuning control, back-end and front-end DC/DC converter, and different compensation topologies [1, 10, 11]. An IPT-based charging system generally consists of three sub-circuitries: the high frequency (HF) inverter, the loosely magnetic coupled transformer and the compensation networks [12].

In IPT charging systems, the compensation networks are very important for the overall performance since they constitute resonant tanks with loosely connected inductors to decrease the system's VA rating while increasing power transfer capabilities [6].

The system phase and frequency responses under CC and CV modes are different. By the compensation topology, the system's input impedance can be made independent of the nonlinear load characteristic of batteries. That requires providing zero phase angle (ZPA) of the impedance. Therefore, the overall impedance acts like a resistor. As a result of that, the voltage-current rating of the power supply can be reduced during the charging process, which decreases power transfer losses and eliminates power stress on the HF inverter. [13, 14].

Various compensation circuitries, such as basic and high-order types under different load levels, have been investigated in the literature [15]. Based on the location and connection types of the resonant capacitors, the basic compensation topologies can be divided into four categories: series-series (SS), series-parallel (SP), parallel-series (PS) and parallel-parallel (PP) [16, 17]. However, these four compensated topologies have limited design parameters and cannot simultaneously assure the unity power factor with ZPA for both CC and CV modes [18]. To overcome these drawbacks of the four basic compensation topologies, high-order compensation circuitries are introduced, such as LCL, Double-sided LCC, LCC-P, LLC-P and LCCL-S.

In a double-sided LCL topology, the magnitude of the output voltage can be regulated using phase modulation techniques [19]. However, the design of an LCL topology requires additional capacitors and inductors on the transmitter and receiver sides of the transformer.

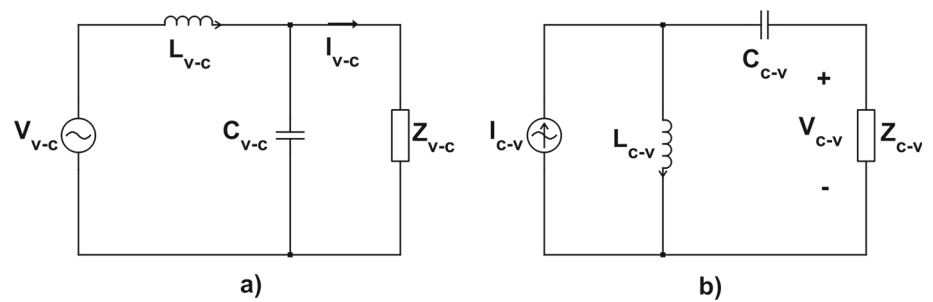
Different LCC topology can also perform CC and CV charging modes with ZPA conditions by its single circuitry. It also allows flexibility to adjust configuration parameters [2, 20]. LCC circuit structure is designed by adding a capacitor into LCL topology, located in series with a transmitter and/or receiver coil in LCL circuitry. The LCC topology not only provides the same advantages as the LCL, but it also results in the freedom of tuning resonance frequencies

for the system. The double-sided LCC (or LCC-LCC) has received significant attention due to its constant current output characteristic, low voltage stress, and excellent efficiency throughout a wide variety of operating range. A double-sided LCC topology with variable coupling coefficient approach is introduced to implement zero-voltage switching (ZVS) in [5]. Furthermore, a double-sided LCC topology is analyzed considering the rectifier equivalent inductance of the rectifier in [21], which makes the circuit to obtain output power closer to the desired level. In [18], another proposed double-sided topology realizes CC and CV modes with reducing AC switches by changing the resonant frequency of the circuit. In [22], an efficient and practical control trajectory is proposed to operate the inverter side of the circuit in half-bridge and full-bridge mode to enable ZVS operation over a wide current range.

Using an LCC compensation tank on the transmitter side is widely preferred in some IPT applications, such as LCC-P and LCC-S types [2]. LCC-P and LCC-S compensation tanks have fewer components on the receiver side than double-sided LCC. An LCC-P compensation topology is proposed for underwater vehicles, including a single capacitor on the receiver side connected in parallel to the receiver coil [11]. An LCC-S topology is realized for CC and CV wireless charging mode with ZPA condition by having two different resonance frequencies in [6]. In [23], an LCC-S circuit is used to perform WPT without any information on the receiver side parameters by using PWM-synchronized samples from the front-end values of the transmitter side of the LCC-S circuit. In [24], another modified LCC-S topology is alternatively presented, which can perform CC and CV charging operations with ZPA through a single switch in two switching frequencies. This approach requires the control circuit complex and makes difficult to eliminate EMI problems. To have a single frequency, another modified LCC-S is also presented for CC and CV charging modes by connecting capacitance in series on the receiver side by two AC switches in [25]. The LCC-P and LCC-S have not only the same advantages of the double-sided LCC topology, but also they reduced size and lower the cost due to requiring fewer components on the receiver side than double-sided LCC topology. In [26], a modified hybrid topology based on double-sided LCC and LCC-S is presented, which performs CC and CV modes with ZPA by modifying circuit types through two AC switches. In [27], the tolerances of LCC-P and LCC-S are compared for the misalignment condition for the pads of the transformer. It was found that LCC-P demonstrates better resistance offsets, while LCC-S can achieve ZPA, and it reduces the reactive part of the input power.

Additionally, higher-order compensation topologies such as LCCL-S have also been studied to improve power transfer efficiency and lead system design freedom. In [28], the performance of the SS and LCCL-S topology is compared

Fig. 1 Resonant network configurations. **a** V-C type, **b** C-V type



in terms of the output characteristics and power transfer efficiencies in both tuning and disrupting states. The results show that the LCCL-S have higher efficiency power transfer at lower power levels. In [29], the output characteristics of SS and LCCL-S topologies are also analyzed for different voltage gain levels.

Over existing studies, this research proposes a novel hybrid topology based on the SS and LCC-S circuitries, including a variable inductor. Unlike the studies discussed in [6] and [25], the proposed system performs CC and CV modes with load-independent ZPA condition at a single resonant frequency by using single AC switches without varying resonant frequency for CC and CV modes. Moreover, the proposed topology includes fewer capacitors to achieve ZPA condition in both charging modes at a single resonant frequency compared to [21] and [26]. Hence, this leads the topology to extend the circuit’s lifespan due to reduced capacitor usage. In the proposed topology, a tunable inductor is introduced, and it is connected in parallel with the series capacitor as a novelty of the study. Besides that, a single switch is connected in series with the input parallel capacitor on the primary side of the circuit to implement the CC and CV modes at a single resonant frequency. Hence, the operating frequency of the proposed IPT systems was fixed throughout all charging modes, reducing the problems caused by frequency hopping. Also, this provides reduced complexity and low-cost circuitry compared to the other existing topologies, which use two or more ACSs to realize CC or CV mode at the same frequency.

The rest of the manuscript is organized as follows: Section 2 introduces a detailed analysis of each operation mode for the SS and LCC-S topology based on the transformer π model. The design consideration for the implementation of the proposed topology is mentioned in Section 3. In Section 4, analytical results are validated via simulations using a 2.4 kW modified hybrid topology, and a comprehensive topology comparison is discussed in detail. Finally, the conclusions are summarized in Section 5.

2 Theoretical analysis of the proposed circuit

In an IPT system, reducing the VA rating of the dc source is the fundamental criterion of the resonant network structure. On the receiver side, the resonant network adjusts the secondary coil’s inductance to enhance transmission capabilities. In general, inductors and capacitors are the two main components found in resonant networks. In IPT systems, LC and CL resonant networks are frequently applied [24]. The type of AC power source, such as an AC voltage source (ACVS) or an AC current source (ACCS), that is supplied to the particular resonant network determines the significance of the CV or CC output characteristics to the load impedance Z in these passive resonant networks [25]. Hereby, Fig. 1 shows two types of the several passive resonant networks, which provide CC and CV output possible for IPT applications.

Figure 1a presents a V–C type resonant network, where the resonant frequency is the same as the angular frequency (ω_{v-c}) of the input AC voltage source and can be defined as in Eq. (1).

$$\omega_{v-c} = \frac{1}{\sqrt{L_{v-c}C_{v-c}}} \tag{1}$$

Based on Kirchhoff’s voltage law (KVL) and Kirchhoff’s current law (KCL), the passive resonant current output in Fig. 1a can be given as in Eq. (2).

$$I_{v-c} = -jV_{v-c}\sqrt{\frac{C_{v-c}}{L_{v-c}}} = -j\frac{V_{v-c}}{\omega_{v-c}L_{v-c}} \tag{2}$$

In (2), V_{v-c} represents the input voltage of the V–C resonant network and I_{v-c} is the value of the output current of the network circuit. According to (2), if the RMS value of V_{v-c} is constant, the circuit operates at resonance frequency as well, I_{v-c} is independent of Z_{v-c} . Thus, the V–C resonant network shows CC output characteristic.

Additionally, the C–V passive resonant network presented in Fig. 1(b) has similar analytic procedures when the resonant frequency of the C–V network is the same as the angular frequency (ω_{c-v}) of the input AC current source and can be defined as in Eq. (3).

$$\omega_{c-v} = \frac{1}{\sqrt{L_{c-v}C_{c-v}}} \quad (3)$$

On the basis of Kirchhoff's voltage law (KVL) and Kirchhoff's current law (KCL), the passive resonant voltage output in Fig. 1b can be given as in Eq. (4).

$$V_{c-v} = jI_{c-v} \sqrt{\frac{L_{c-v}}{C_{c-v}}} = j\omega_{c-v}L_{c-v}I_{c-v} \quad (4)$$

In (4), I_{c-v} is the input current of the C–V resonant network and V_{c-v} is defined as the output voltage of the network circuit. According to (4), if the RMS value of I_{c-v} is constant, the circuit operates at resonance frequency as well, V_{c-v} is independent of Z_{c-v} . Therefore, the C–V resonant network presents CV output characteristic. As a result, the resonant frequency of the V–C network is adjusted as the resonant frequency of the V–C network to provide the CC and CV output characteristic for the designed IPT topology:

$$\omega_{v-c} = \omega_{c-v} \quad (5)$$

2.1 Analysis of the proposed hybrid topology

As discussed earlier, the LCC-S topologies perform better efficiency by applying the ZPA condition in lower power condition and are used in reducing reactive power. However, SS topologies demonstrate better performance for high-power applications [29]. Hence, SS and LCC-S-based hybrid topologies have become widely preferred in the literature. They include the SS and LCC-S advantages, such as better efficiencies for high and low power conditions and CC/CV charging mode with ZPA ability. In [6], SS combined with LCC-S performs ZPA conditional CC and CV operations without using any switches at two different resonant frequencies. However, another SS and LCC-S-based topology is demonstrated in [25], with ZPA capable of performing the CC and CV charge modes at the same resonant frequency, but using a total of two AC switches on each side of the circuit.

In this study, a modified IPT topology, derived from [6] and [25], is demonstrated by adding a tunable inductor to the primary side of the circuit. The proposed topology can perform each charging operation at the same resonant frequency and also includes only one AC switch on the primary side to select CC or CV operation depending on the equivalent battery load. The structure of the proposed WPT system based on

the modified hybrid topology is shown in Fig. 2. The mutual inductance is M , and the inductances of the transmitter and receiver coils are L_p and L_s , respectively. C_p is the parallel compensation capacitor, L_{in} is the series compensation inductor, C_f is the series compensation capacitor, L_x is the adjustable shunt inductor connected in parallel with the C_f , and C_s is the series compensation capacitor on the receiver side. Additionally, the proposed circuit includes a full-bridge inverter at the input of the transmitter stage, a rectifier at the output of the receiver stage and an extra AC switch (ACS) (S_5) used to switch between the CC and CV charging modes of the circuit.

Also, the First Harmonic Approximation (FHA) is used to analyze the circuit in the frequency domain. A 50% percent fixed duty ratio control signal is used to regulate the switches on the inverter side in Fig. 2 to achieve maximum fundamental output voltage. T-model can accomplish load-independent voltage output and load-independent current output, respectively, when the input source is a sinusoidal voltage source and the aforementioned particular conditions are met. The T-model AC equivalent circuit of the suggested topology is also shown in Fig. 3 to make circuit analysis easier [18].

The primary and secondary sides of the coils are considered to be equal for the sake of simplicity. The leakage inductance of the transmitter and receiver side coils is defined as L_T and L_R . Using the relationships between the self-inductances L_p and L_s , the coupling coefficient factor k can be stated as Eq. (6), where M represents mutual inductance [18].

$$k = \frac{M}{\sqrt{L_p L_s}} \quad (6)$$

T-model parameters such as L_T and L_R leakage inductances can also be calculated as follows [1]:

$$\begin{cases} L_T = L_p - M \\ L_R = L_s - M \end{cases} \quad (7)$$

In most WPT systems, the compensation circuits have very high-quality factors. As a result, the input current and voltage harmonics are relatively low. Therefore, FHA can be employed in mathematical analysis without error [25]. The first-order harmonics based on the circuit model illustrated in Fig. 3 can be produced using FHA as in Eq. (8) [18].

$$\begin{cases} v_{AB}(t) = \frac{4}{\pi} V_{in} \sin(2\pi f t) \\ v_{ab}(t) = \frac{4}{\pi} V_o \sin(2\pi f t + \theta) \\ i_{ab}(t) = \frac{\pi}{2} I_o \sin(2\pi f t + \theta) \end{cases} \quad (8)$$

The input DC voltage, output charging voltage, and current are represented by the variables V_{in} , V_o and I_o , respectively. θ is the degree of the phase difference between v_{AB} and

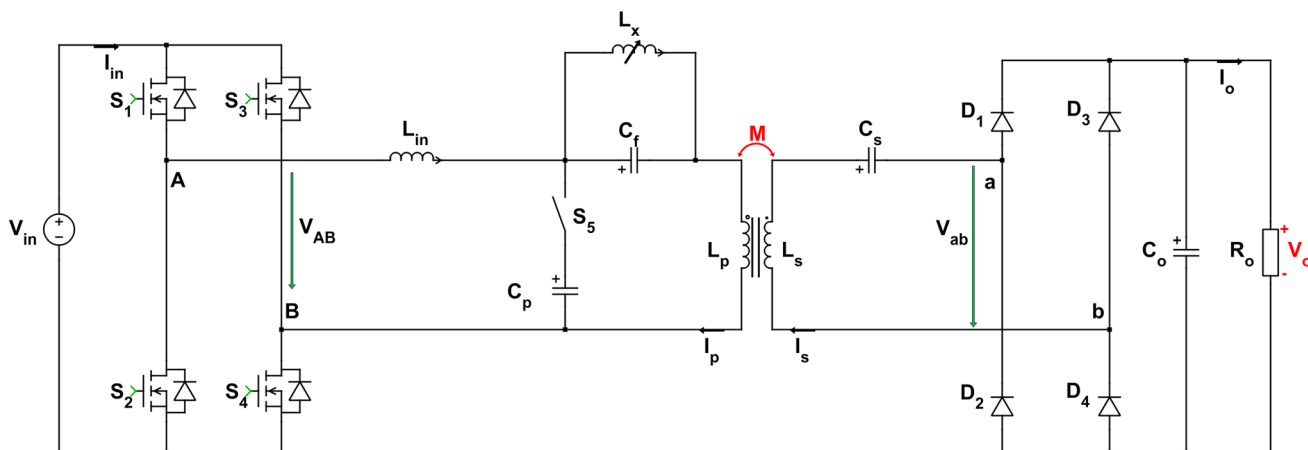


Fig. 2 Proposed LCC-based compensation topology circuit

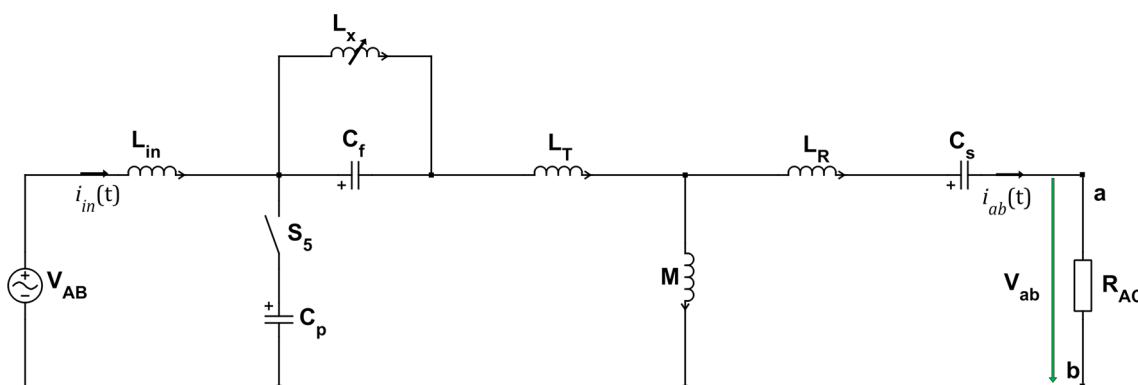


Fig. 3 T-model AC equivalent circuit of the proposed topology

v_{ab} . On the receiver side, the bridge rectifier using $D_1 \sim D_4$ diodes converts the AC output voltage (V_{ab}) and current (I_s) to the battery charging DC voltage (V_o) and current (I_o) [25]. However, since the output low-pass filter only has one capacitance (C_o), the relationships between the AC output voltage and current and the battery voltage and current can be stated in Eqs. (9) and (10), respectively [30].

$$V_o = \frac{\pi\sqrt{2}}{4} V_{ab} \tag{9}$$

$$I_o = \frac{2\sqrt{2}}{\pi} I_s \tag{10}$$

V_{ab} and I_s are the RMS values of V_{ab} and I_s , respectively. Depending on Eqs. (9) and (10), the output AC equivalent resistance (R_{AC}) depending on battery resistance can be defined as in Eq. (11) according to [28].

$$R_{AC} = \frac{8}{\pi^2} R_o \tag{11}$$

In the following sections, the proposed hybrid topology is theoretically investigated to examine how to perform CC and CV charging operations for the load-independent condition.

2.2 CC Mode Implementation of the Proposed Hybrid Topology

In the case of CC charging mode, the S_5 is switched off, as shown in Fig. 3. Also, each component’s parasitic resistance is ignored. Therefore, the proposed hybrid circuit converts to the SS compensation topology. Figure 4 depicts the equivalent T model circuit for the CC mode charging, where $L_{p'}$ represents the equivalent series inductance of L_p and L_{in} defined as (12).

$$L_{p'} = L_p + L_{in} = L_T + M + L_{in} \tag{12}$$

In CC charging mode, the parallel connection of L_x and C_f is regarded as an equivalent capacitance $C_{f'}$ when the value of C_f is large enough, according to [1].

$$C_{f'} = \frac{\omega_{cc}^2 L_x C_f - 1}{\omega_{cc}^2 L_x} \tag{13}$$

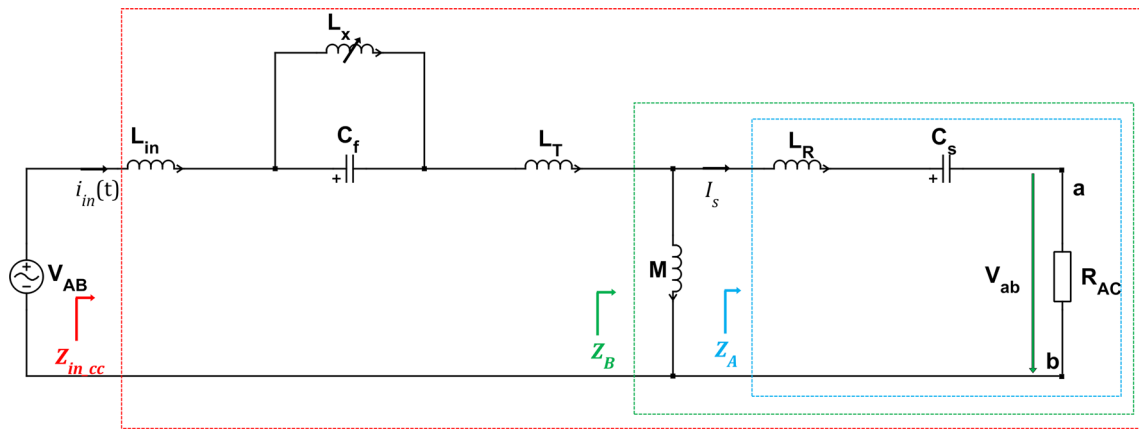


Fig. 4 Simplified equivalent T-model in CC mode charging

To achieve ZPA condition for the CC mode in the transmitter side of the topology regardless of the load, the $C_{f'}$ must be selected to resonate with $L_{p'}$. Depending on this requirement, the following equations must be satisfied:

$$0 = j \left(\omega_{cc} L_{p'} - \frac{1}{\omega_{cc} C_{f'}} \right) \tag{14}$$

$$\omega_{cc}^2 = \frac{1}{L_{p'} C_{f'}} \tag{15}$$

As discussed above, $C_{f'}$ resonates with $L_{p'}$ to eliminate the imaginary part of input impedance (Z_{in_cc}). Therefore, the current of the receiver coil (I_s) is calculated as in (16) based on the Kirchhoff’s voltage and Kirchhoff’s current laws for Z_{in_cc} , according to [1]:

$$I_s = -j V_{AB} \sqrt{\frac{C_{f'}}{M}} = \frac{V_{AB}}{j \omega_{cc} M} \tag{16}$$

Under the CC mode, I_o can be calculated by substituting Eq. (16) in Eq. (10) according to [1]:

$$I_o = \frac{2\sqrt{2}}{\pi} I_s = \frac{2\sqrt{2} V_{AB}}{\omega_{cc} \pi M} \tag{17}$$

Hence, the transconductance gain (G_T) for the CC charging mode regardless of the load can be derived as (18):

$$G_T = \frac{I_o}{V_{AB}} = \frac{2\sqrt{2}}{\omega_{cc} \pi M} \tag{18}$$

The impedance parameters described in Fig. 4, according to the proposed LCC circuit, are given as follows:

$$Z_A = R_{AC} + \frac{1}{j \omega C_s} + j \omega L_R \tag{19}$$

$$Z_B = \frac{Z_A j \omega_{cc} M}{Z_A + j \omega_{cc} M} \tag{20}$$

Moreover, the input impedance of the proposed topology is required to detect the ZPA condition in CC charging mode. Therefore, the input impedance (Z_{in_cc}) of the proposed topology can be calculated as (21) depending on Z_A and Z_B impedance parameters.

$$Z_{in_cc} = Z_B + \frac{1}{j \omega C_{f'}} + j \omega L_T + j \omega L_{in} \tag{21}$$

To conduct ZPA at the resonant frequency, the phase angle of the input impedance (θ_{in_cc}) must be equal to zero. The input phase angle of the proposed topology is defined as (22). In this manner, zero-voltage switching can be adequately achieved for the CC mode.

$$\theta_{in_cc} = \frac{180^\circ}{\pi} \tan^{-1} \left[\frac{Im(Z_{in_cc})}{Re(Z_{in_cc})} \right] = 0 \tag{22}$$

2.3 CV mode implementation of the proposed hybrid topology

In Fig. 3, the whole circuit model of the proposed topology is demonstrated. When the S_5 is switched on, the T-model corresponding circuit for the CV mode shown in Fig. 5 transforms to the LCC-S topology. The transmitter coil current I_p is computed as follows to guarantee that L_{in} resonates with C_p .

Based on the Kirchhoff’s voltage and Kirchhoff’s current laws, the current of the transmitter coil is defined as in Eq. (23) according to [25]:

$$I_p = -j V_{AB} \sqrt{\frac{C_p}{L_{in}}} = -j \frac{V_{AB}}{\omega_{cv} L_{in}} \tag{23}$$

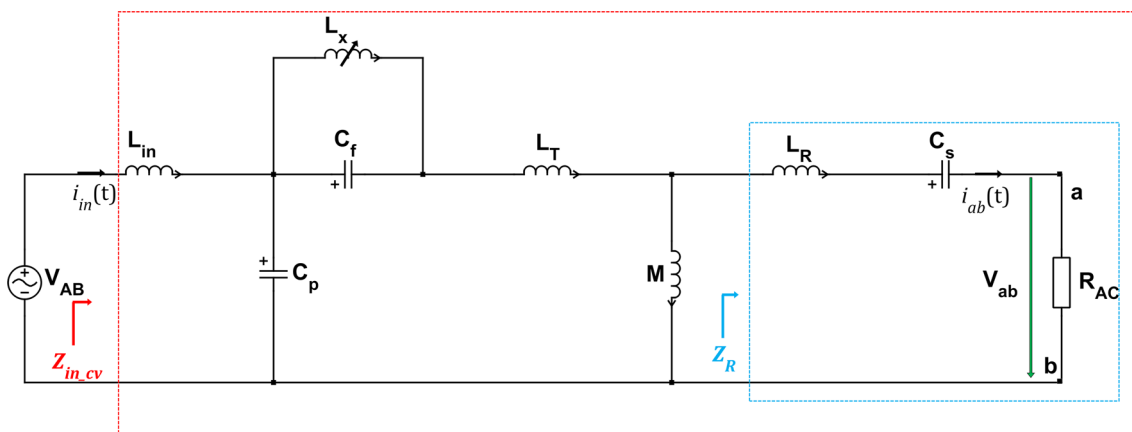


Fig. 5 Simplified equivalent T-model in CV mode charging

Under constant V_{AB} and L_{in} , the primary current I_p has a fixed value and is regardless of the parameters. To achieve ZPA condition for the CV mode in the receiver side of the topology regardless of the load, the C_s must be selected to resonate with L_s . Depending on this requirement, the following equations must be satisfied:

$$0 = j\left(\omega_{cv}L_s - \frac{1}{\omega_{cv}C_s}\right) \tag{24}$$

$$\omega_{cv}^2 = \frac{1}{L_s C_s} \tag{25}$$

$$V_{ab} = j\omega M I_p = \frac{M V_{AB}}{L_{in}} \tag{26}$$

Therefore, the voltage gain (G_V) for the CV charging mode regardless of the load can be derived as (27):

$$G_V = \frac{V_{ab}}{V_{AB}} = \frac{M}{L_{in}} \tag{27}$$

Moreover, the receiver side impedance can be calculated as in (28).

$$Z_R = j\omega_{cv}L_R - j\frac{1}{\omega_{cv}C_s} + R_{AC} \tag{28}$$

Using Eq. (28), the input impedance Z_{in_cv} of the simplified equivalent T – model of the proposed LCC topology shown in Fig. 5 can be calculated as in (29):

$$Z_{in_cv} = \left(\left[(Z_R || j\omega_{cv}M) + \left(j\omega_{cv}L_T + \frac{1}{j\omega_{cv}C_{f'}} \right) \right] || \left[\frac{1}{j\omega_{cv}C_p} \right] \right) + (j\omega_{cv}L_{in}) \tag{29}$$

Also, the input impedance in CV mode Z_{in_cv} at ZPA can be calculated using the condition indicated in Eq. (21) and Eq. (9) when combined with Eq. (9) as follows:

$$Z_{in_cv} = \frac{8 L_{in}^2 R_o}{\pi^2 M^2} \tag{30}$$

Additionally, the phase angle (θ_{in_cv}) of the input impedance must be equal to zero to perform ZPA at the resonant frequency. Therefore, the input phase angle of the proposed topology in CV mode is defined as in Eq. (31). In this manner, the zero-voltage switching can be achieved properly for the CV mode.

$$\theta_{in_cv} = \frac{180^\circ}{\pi} \tan^{-1} \left[\frac{Im(Z_{in_cv})}{Re(Z_{in_cv})} \right] = 0 \tag{31}$$

3 Design procedures of the topology parameters

In general, compensation circuit parameters are important factors that influence the IPT system’s efficiency, output characteristics, and voltage/current stress [28]. The converter operates in the ZPA state when the resonant circuit parameters are designed according to the previous requirements. Therefore, the parameter design technique for the proposed switching hybrid compensation topology’s CC/CV output implementation is detailed below. As presented in Fig. 3, the proposed topology is composed of the SS and LCC-S compensation topology. To achieve the CC and CV charging modes, a tunable L_x inductor is connected in parallel to the C_f and an additional S_5 ACS is attached in series to the parallel capacitor on the primary side of the circuit. When S_5 is turned on, as shown in Fig. 4, the proposed circuit forms to LCC-S topology, which performs CV charging mode at the

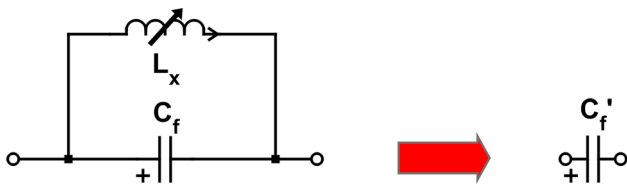


Fig. 6 Equivalent circuit scheme for $C_{f'}$ with the parallel connection of L_x and C_f

Table 1 Specifications of the IPT battery charger

Parameters	Description	Rate
P_o	Power rating	2.4 kW
V_{in}	Input voltage (DC)	350 V
V_o	CV mode output voltage	400 V
I_o	CC mode output current	6 A

same resonant frequency as CC charging. Also, the equivalent capacitance values of $C_{f'}$ satisfying Eqs. (21) and (29) must be calculated for the ZPA condition in CC and CV mode, respectively.

When the value of C_f is big enough, the parallel connection of L_x and C_f is regarded as an equivalent capacitance $C_{f'}$. As a result, as illustrated in Fig. 6, L_x and C_f are connected in parallel to fulfill the needed value of $C_{f'}$ for the ZPA requirement.

In order to achieve ZPA condition for each charging modes, the tunable L_x must be adjusted to meet the proper value of $C_{f'}$. Accordingly, the tunable L_x inductor value should be calculated for each charging mode depending the required value of $C_{f'}$ as defined in Eq. (32).

$$L_x = \frac{1}{\omega^2(C_f - C_{f'})} \quad (32)$$

In this paper, a 2.4 kW WPT system is designed to implement the proposed topology circuit. The proposed system operates with a fixed frequency of 85 kHz for the CC and CV charging modes. The input DC voltage (V_{DC}) is 350 V, and the required battery current is 6 A. When the battery's voltage exceeds 400 V, the charging mode switches from CC to CV. At this point, the S_5 is turned on and L_x inductor value is changed, which satisfies the ZPA condition for the CV mode. Table 1 lists the required output qualities of the studied IPT charging. In addition, The CC/CV charging curve and equivalent impedance of the Li-ion battery utilized in this work are shown in Fig. 7.

Depending on the IPT coupler side and coil geometry of the existing transformer, which is planning to be used for this study, the self-inductance value of each coil is measured as 252 μ H for the primary and 244.6 μ H for the secondary side.

From Eq. (18), the transconductance gain (G_T) in CC mode can be calculated as follows:

$$G_T = \frac{I_s}{V_{in}} = \frac{I_o \times 2\sqrt{2}}{V_{in} \times \pi} \approx 0.02 \quad (33)$$

Using the IPT charger specifications presented in Table 1, the mutual inductance from Eq. (18) is calculated as follows:

$$M = \frac{2\sqrt{2}}{\omega_{cc}\pi G_T} \approx 89 \mu\text{H} \quad (34)$$

Then, L_{in} can be determined from the voltage gain (G_V) in the CV charging mode shown in Eq. (26) as follows:

$$L_{in} = \frac{M}{G_V} = \frac{M \times V_{in}}{V_{out}} \approx 78.7 \mu\text{H} \quad (35)$$

Additionally, the serial capacitor value of the secondary part (C_s) can be obtained from Eq. (25) as follows:

$$C_s = \frac{1}{L_s \omega_{cv}^2} \approx 14.33 \text{ nF} \quad (36)$$

In Fig. 7, four operation points (25 Ω , 67 Ω , 90 Ω and 200 Ω) are selected due to observing the all over the performance of the proposed design. To realize the required battery charging conditions, the prototype's designed circuit resonant circuit parameters are listed in Table 2.

However, the circuit parameters must be determined to implement the ZPA in CC and CV mode charging at the same resonant frequency. The imaginary components of Eqs. (21) and (29) should be set to zero to achieve ZPA for both charging modes. Depending on the specifications in Table 2, also, $C_{f'}$ is determined as 10.6 nF for the CC mode and 20.23 nF for the CV mode. Hence, the tunable L_x inductor value can be calculated by using Eq. (32) for both modes as follows:

$$L_{x(cc)} = \frac{1}{(2\pi \times 85)^2 \times (30 - 10.6) \times 10^{-9}} \cong 180 \mu\text{H} \quad (37)$$

$$L_{x(cv)} = \frac{1}{(2\pi \times 85)^2 \times (30 - 20.23) \times 10^{-9}} \cong 360 \mu\text{H} \quad (38)$$

Moreover, the value of each circuit component is necessary to be calculated depending on the desired output current–voltage levels and selected resonant frequency. Hence, the design procedures to determine component values require some calculating iterations, as presented in Fig. 8, to meet the required CC and CV modes for the better charging. To calculate the exact values of the component parameters, a

Fig. 7 CC/CV charging profile and equivalent circuit of the used Li-ion battery

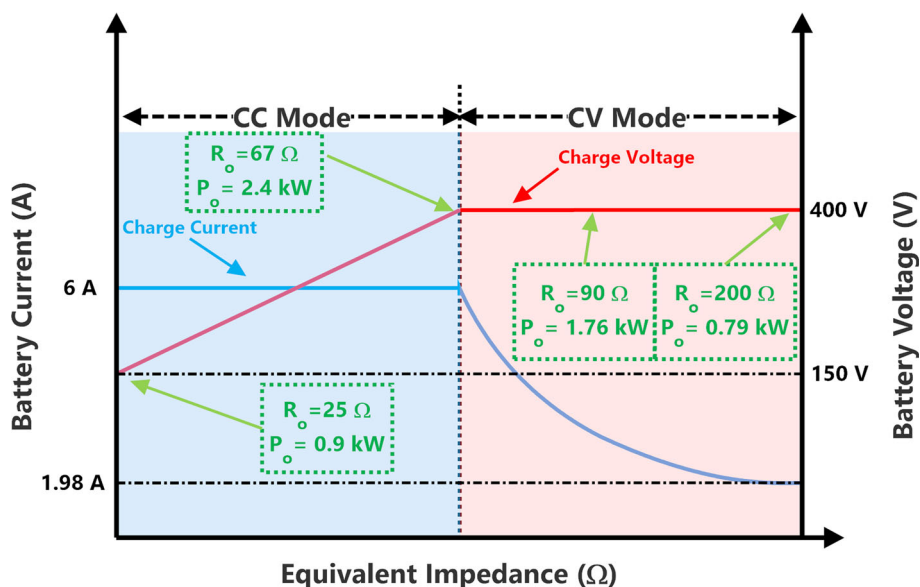


Table 2 Component parameters of the designed hybrid topology

Parameters	Description	Rate
L_{in}	Primary series inductor	78.7 μ H
C_p	Primary parallel capacitor	44.54 nF
C_f	Primary serial capacitor	30 nF
C_s	Secondary serial capacitor	14.33 nF
f_{cc}, f_{cv}	Frequency in CC and CV mode	85 kHz
M	Mutual inductance	89 μ H
L_p	Primary coil self-inductance	252 μ H
L_s	Secondary coil self-inductance	244.6 μ H
k	Coupling coefficient	0.3585

feasible flowchart for the proposed hybrid topology is illustrated in Fig. 8 to perform the CC charge with the following CV charge profile.

However, the battery equivalent load changes the entire charging process, affecting the efficiency of the whole topology. Therefore, in the topology design, the input impedance should be adjusted to be independent of the equivalent load, and the reactive power component should be minimized. Hence, this provides to reduce the switching losses of the inverter side of the circuit and improves system performance for each charging process. To verify the proposed design, a mathematical analysis was performed referring to the circuit parameters listed in Table 2. In this context, Fig. 9 depicts the transconductance gain (G_T) and the input phase angle ($\theta_{in_{cc}}$) under the CC charging mode for various load conditions of 20 Ω , 40 Ω , 60 Ω and 80 Ω at different frequencies. Figure 10 shows the voltage gain (G_V) and the input phase angle ($\theta_{in_{cv}}$) at different frequencies under the CV charging

mode. Figures 9b and 10a show that G_T and G_V are constant at the same at 85 kHz regardless of the load for the CC and CV modes, respectively.

As demonstrated in Fig. 9c and Fig. 10c, the phase of the input impedances equals to zero for both charging modes. And, it provides fixed current and voltage output levels regardless of the battery load at the 85 kHz resonant frequency. Thus, ZPA is achieved successfully for each charging mode at the same operating frequency, which improves system efficiency and VA rating of the designed topology.

4 Simulation results and system topology comparison

4.1 Simulation results

A model of 2.4 kW IPT was created to simulate and verify theoretical results for CC and CV operation modes to confirm the investigated hybrid topology circuit and designs. In the simulation study, a DC voltage source with 350 V input was used as the input of the proposed hybrid topology, and the assigned battery charge voltage (V_o) and current (I_o) values are 400 V and 6 A, respectively. Furthermore, the proposed circuit is built to provide the maximum power for the critical charging point between CC and CV modes.

Consequently, Fig. 11 depicts the proposed hybrid topology, which is built using the parameters stated in Table 2. Also, the required simulation analysis was realized in PLECS with MATLAB/Simulink environment between CC and CV modes, referring to Table 2. To be more accurate to the real application of the circuit, non-ideal switches, transformers and inductors are utilized in the simulation. The output power

Fig. 8 The flowchart to specify the topology parameters of the proposed system

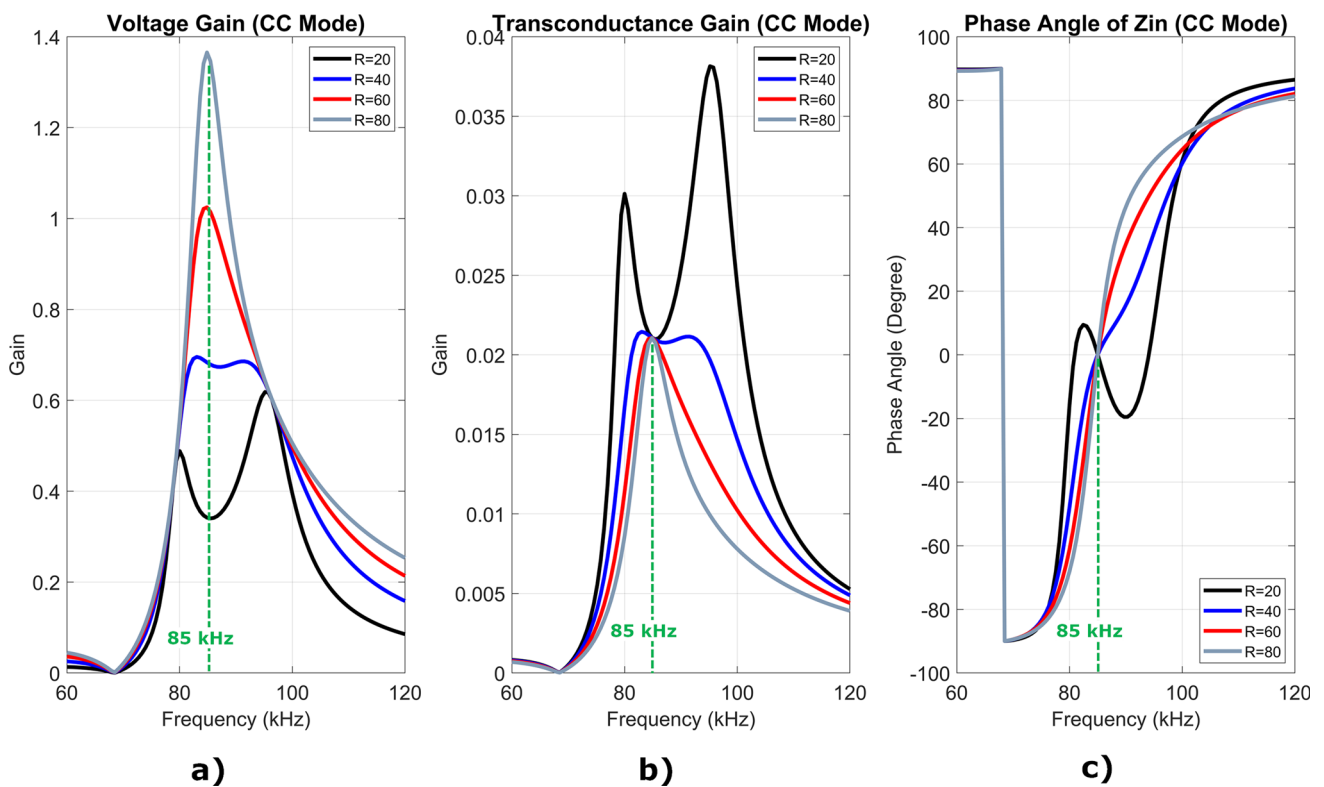
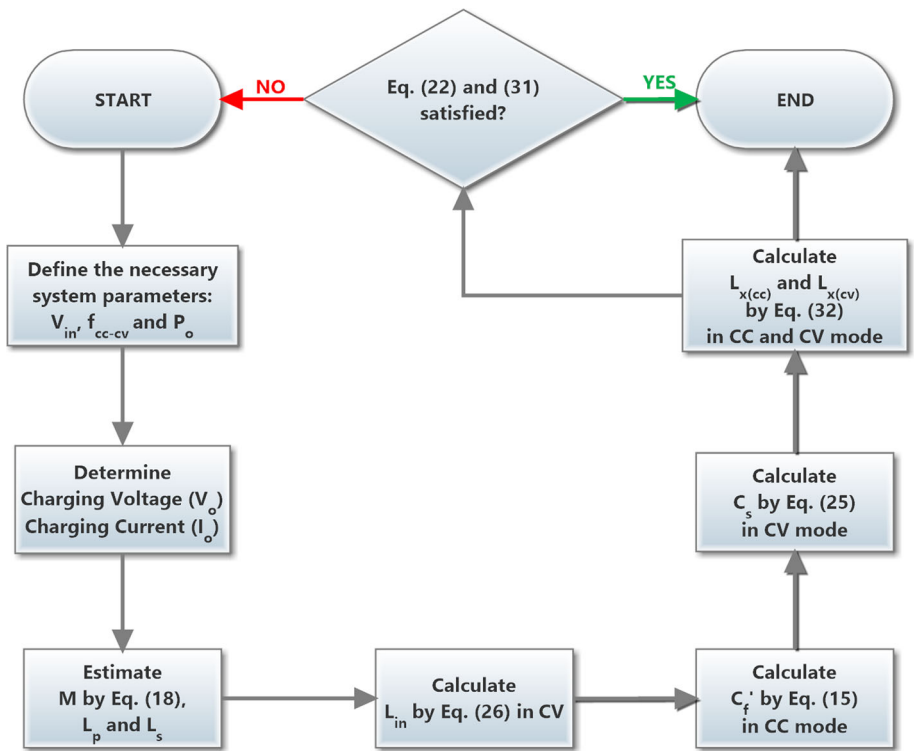


Fig. 9 **a** Voltage gain (G_V), **b** transconductance gain (G_T), **c** phase angle ($\theta_{in,cc}$) of the proposed topology for the CC mode

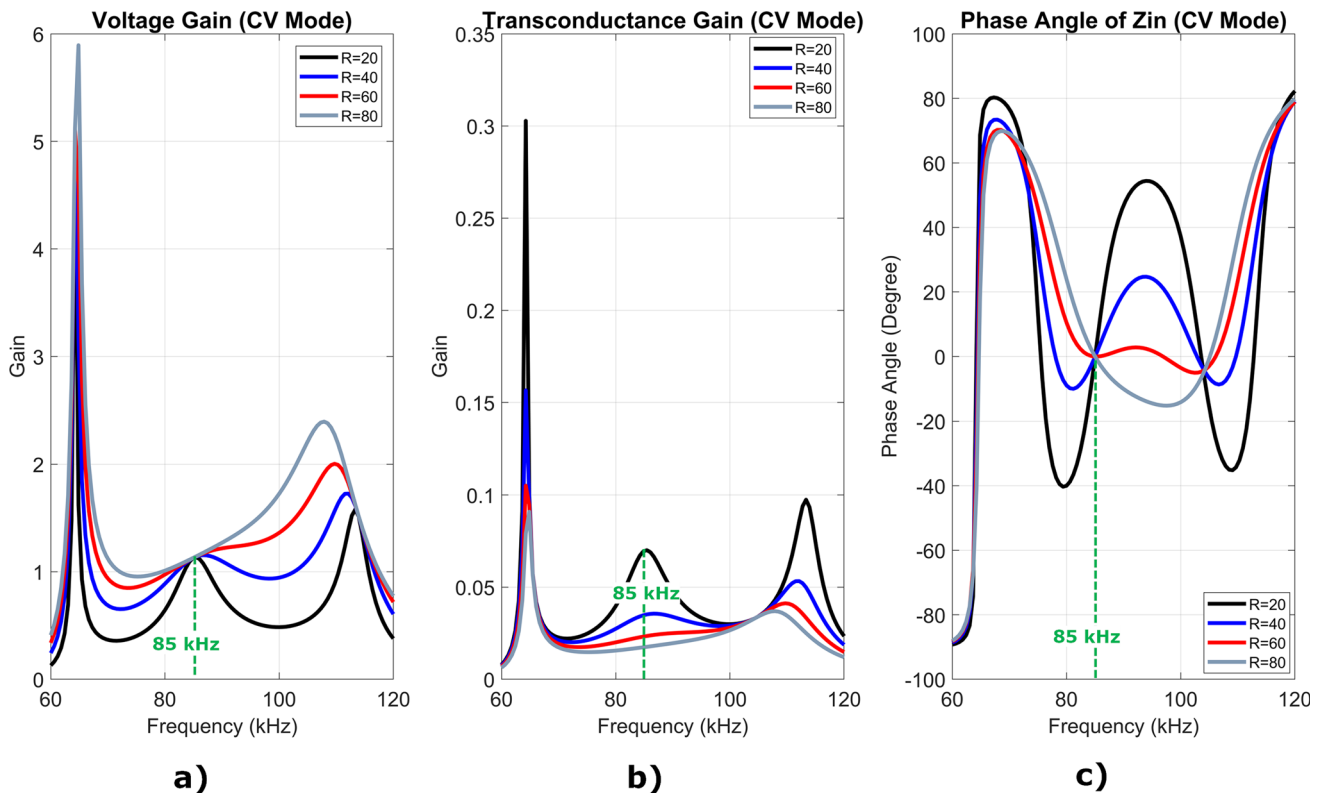


Fig. 10 a Voltage gain (G_V), b transconductance gain (G_T), c phase angle (θ_{in_cv}) of the proposed topology for the CV mode

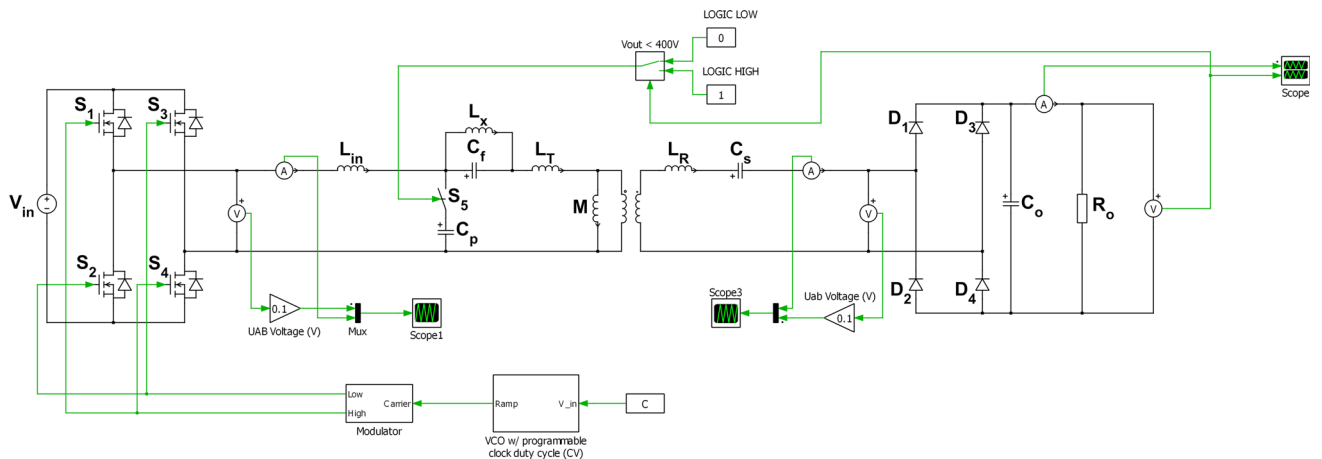


Fig. 11 Simulation setup for the proposed LCC compensation topology

and system efficiency achieved for various battery resistance values are assessed in this manner. According to the topology’s mathematical analysis, the ZPA condition is satisfied for both CC and CV modes at a single resonant frequency of 85 kHz, as shown in Fig. 9 and Fig. 10.

As illustrated in Fig. 11, the proposed topology contains a single ACS, which generally consists of two series-opposite connected MOSFETs in the WPT applications. In addition, the operating mode of the circuit changes according to whether S_5 is logically high or low, and its logic state is

selected as on or off by detecting the battery output voltage. When the output voltage is measured below as 400 V reference voltage, the logic state becomes logic low, and S_5 is turned off. Otherwise, the S_5 becomes logic high and turned on. The control signal waveform of S_5 is presented in Fig. 12.

To obtain variable inductor, there are different ways such as changing the ferromagnetic core operating points [31] or relay-controlled inductor. For simplicity, the second control approach is implemented. The tunable L_x inductor is also controlled in the same trajectory as the S_5 . In this regard,

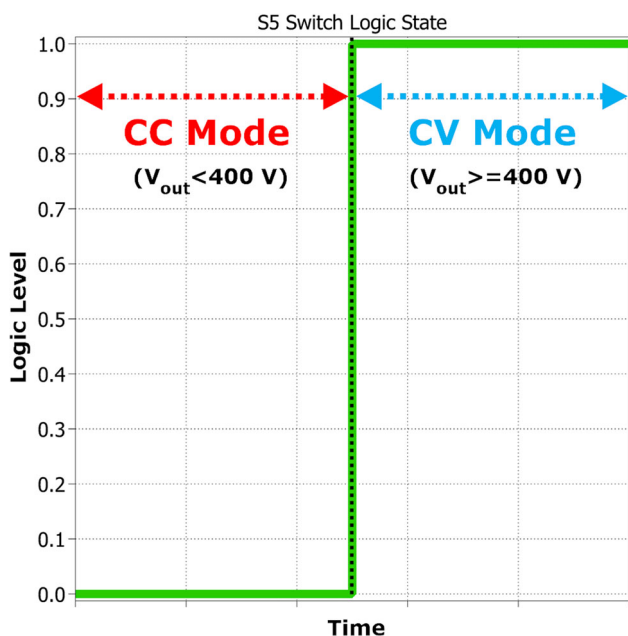


Fig. 12 Logic control waveform for the S_5 in CC and CV modes

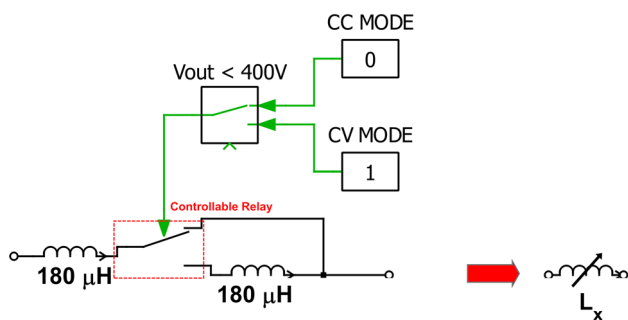


Fig. 13 Equivalent circuit model for the tunable L_x inductor

Fig. 13 shows the equivalent circuit model of the L_x inductor. As presented in Fig. 13, the tunable L_x inductor contains two 180-H inductors and a controllable relay. Depending on the logical state of S_5 illustrated in Fig. 12, the relay is enabled depending on whether CC or CV mode is selected. In CC charging operation, a single 180-H inductor is normally connected to the circuit in parallel with C_f . In CV mode, two 180-H are connected in series in parallel with C_f by activating the controllable relay.

As a result, a detailed control flowchart for controlling the single S_5 ACS switch used in the proposed circuit and the relay used to set the inductor L_x is shown in Fig. 14. As presented in Fig. 14, the suggested controller structure has a straightforward design, making it easy to implement and control. According to the control method, the battery reference voltage is set to 400 V.

In CC charging mode, the S_5 is turned off, and the topology transforms into an SS compensation circuit. Hence, the primary parallel capacitor C_p is disconnected and neglected for

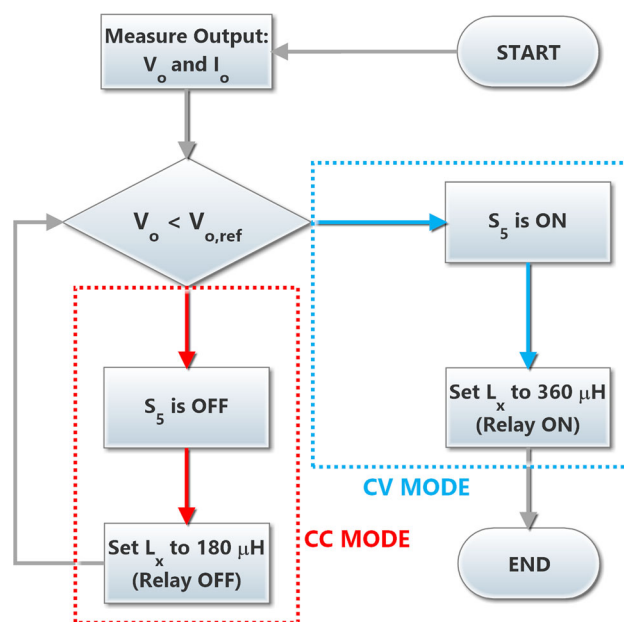


Fig. 14 Flowchart of the CC and CV mode control of the proposed circuit

the CC mode operation. Additionally, the tunable L_x inductor value is set to 180-H . Figure 15 demonstrates the main waveforms of the hybrid LCC circuit for the CC mode charging with 350 V DC input. As observed in Fig. 15a, the I_o charging current remains at 6 A, when the equivalent resistance of the battery (R_o) varies from $25\ \Omega$ to $67\ \Omega$, and the switching frequency remains as same 85 kHz resonant frequency. As a result, the CC mode charging is met for various battery equivalent resistances, as illustrated in Fig. 7. In addition, the input current and voltage waveforms of the hybrid compensation circuit are also shown in Fig. 15b. As investigated in Fig. 15b, the ZPA condition is succeed for the CC charging mode since the zero-voltage-switching (ZVS) condition of the $S_1 \sim S_4$ switches is realized.

In CV charging mode, the S_5 is turned on, and the topology transforms into an LCC-S compensation circuit. Therefore, the primary parallel capacitor C_p is connected in parallel and considered for the CV mode operation. Also, the tunable L_x inductor value is set to 360-H . The proposed LCC circuit's waveforms during CV mode charging with a 400 V DC input are shown in Fig. 16. In CV mode operation, the equivalent resistance varies from 90 to $200\ \Omega$. When the equivalent resistance of the battery (R_o) increases from 90 to $200\ \Omega$, and the output battery charging voltage remains at 400 V, as shown in Fig. 16a. The switching frequency remained constant at 85 kHz, the same as the CC mode resonant frequency. As a result, the CV mode charging is achieved for various output resistances. The input voltage and current waveforms of the hybrid topology are also demonstrated in Fig. 16b. As investigated in Fig. 16b, the ZPA condition is succeed for the

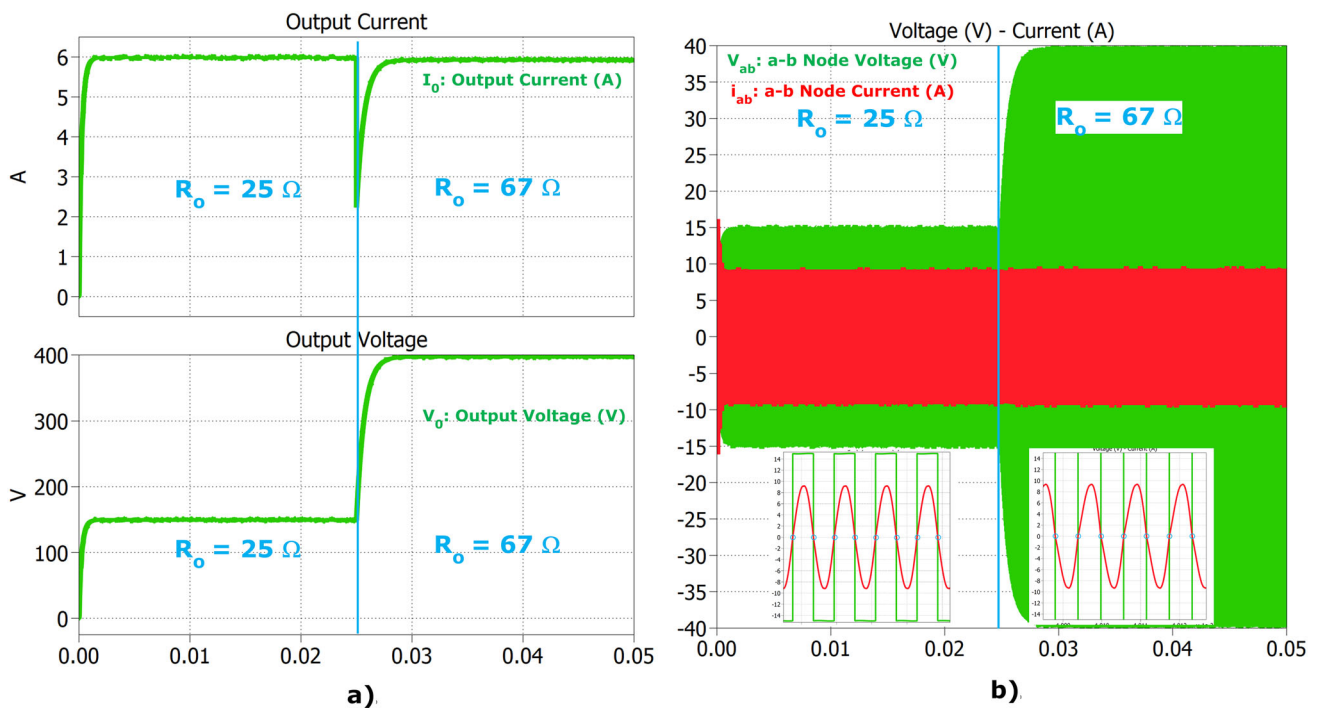


Fig. 15 The CC mode operation waveforms for the LCC circuit, **a** output voltage and current waveforms, **b** input current and voltage waveforms

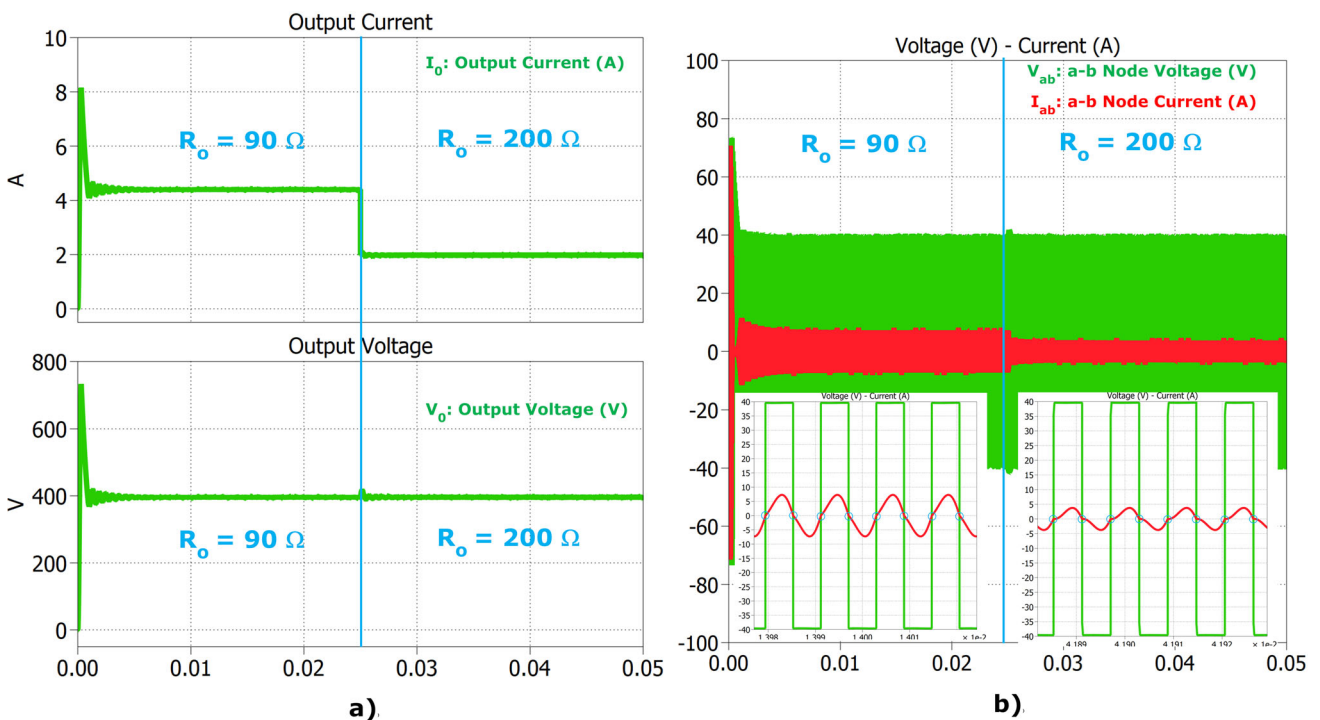


Fig. 16 The CV mode operation waveforms for the LCC circuit, **a** output voltage and current waveforms, **b** input current and voltage waveforms

CV charging mode since the zero-voltage-switching (ZVS) condition of the $S_1 \sim S_4$ switches is realized.

When R_o changes from 25 to 67 Ω in CC mode, the output charge current I_o remains virtually constant while the output charge voltage V_o rises steadily. In the CV charging mode, the

output charge voltage V_o remains almost constant while the output charge current I_o continues to drop, when R_o is varied from 90 to 200 Ω . Furthermore, the ZPA condition is achieved with a nearly zero phase angle. Figures 15 and 16 show the transient waveforms for both CC and CV charging modes as

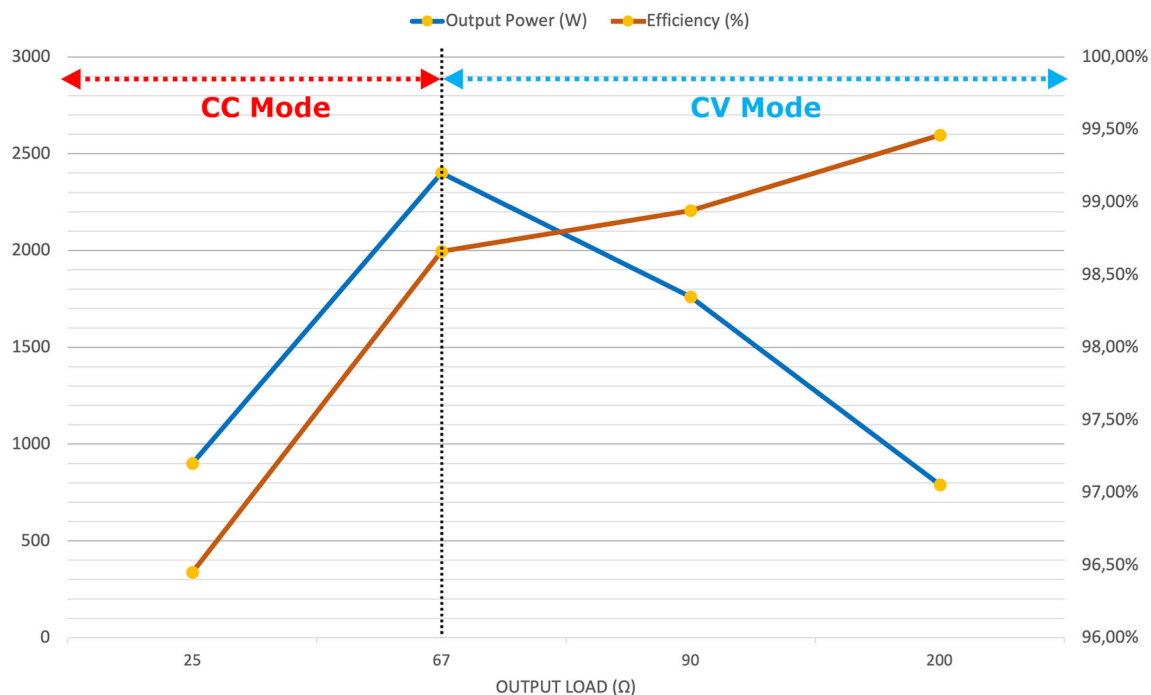


Fig. 17 Overall system efficiency and output power for the CC and CV charging modes

the R_o varies. As a result, the possible significant damages caused by high current/voltage spikes can be avoided due to its fast response time according to the load changes. Hence, the fundamental advantage of the designed hybrid topology is that the CC and CV charging modes can be achieved at a single resonance frequency regardless of the battery load.

Figure 17 presents the overall efficiency and output power in the simulation analysis of the proposed topology for four different loads investigated before. As examined from the efficiency results, it can be observed that the average efficiency of the CV mode is better than the CC mode due to the switching of the circuit from SS to LCC-S topology. At the maximum power of the circuit, the average efficiency is measured as 98.66%, and the output power equals to 2.4 kW approximately. Also, the average efficiency increases as the output load increases in CV mode.

4.2 Effect of coupling factor change

The considerable degree of coil freedom presents a challenge for IPT applications. Therefore, misalignment and distance variations are inevitable between the primary and secondary pads of the transformer. It can also cause undesirable variations in the output voltage and current levels. Consequently, the operation of the designed topology should be examined under varying coupling factors. Therefore, the proposed topology was also examined for various coupling factors, including $k = 0.3$ and $k = 0.4$. For each charging mode, the ZPA condition was also investigated.

Figure 18 depicts the output current and voltage waveforms of the proposed LCC circuit for CC and CV modes with an input voltage of 350 V and a coupling factor of $k = 0.3$. As a result, the output current reaches 7.1 A, as depicted in Fig. 18a, which is slightly greater than the desired 6 A and remains constant regardless of load variations. In addition, the output voltage remains constant regardless of load shown in Fig. 18c. Consequently, the CC and CV modes are attained, albeit at various current and voltage levels. In Fig. 18b and d, current and voltage simultaneously cross the zero point. Therefore, the ZPA condition is specified for both charging phases.

Figure 19 illustrates the waveforms of the proposed LCC circuit for the CC and CV modes with a coupling factor of $k = 0.4$. Figure 19a reveals that the output current approaches 5.37 A, which is lower than the desired 6 A, and remains constant regardless of load variations. In CV mode, as depicted in Fig. 19c, the output voltage remains constant at 441.7 V, which is substantially higher than the 400 V desired value. In Fig. 19b and d current and voltage simultaneously cross the zero point. Therefore, the ZPA condition is specified for both charging phases.

In the simulation analysis of the proposed topology, Fig. 20 depicts the overall efficiency for various coupling factor values, such as 0.3 and 0.4. Due to the misalignment and distance variations of transformer pads, the coupling factor parameter becomes a crucial issue. Examining the efficiency results, it can be seen that the average efficiency for the CV

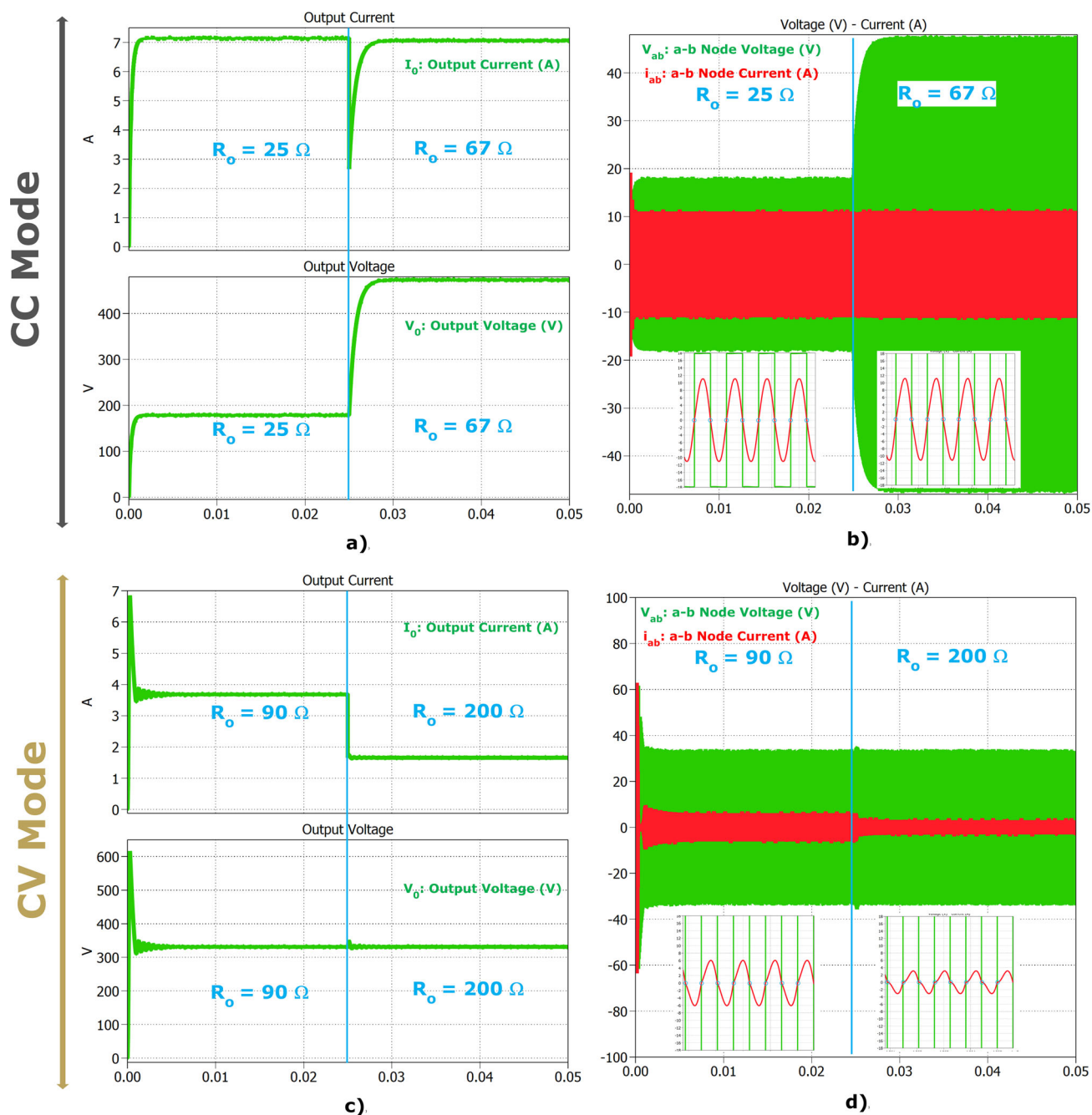


Fig. 18 The output current and voltage waveforms of the LCC circuit for $k = 0.3$ coupling factor, **a** output voltage and current waveforms in CC mode, **b** input current and voltage waveforms in CC mode, **c** output

voltage and current waveforms in CV mode, **d** input current and voltage waveforms in CV mode

and CC modes has nearly remained constant in comparison with its original target value. At the circuit’s maximum power, the average efficacy is measured to be nearly 98.6%. Additionally, as the output load increases in CV mode, the average efficiency increases. Consequently, the average efficacy of the CV mode is greater than that of the CC mode as a result of the circuit’s transition from SS to LCC-S topology.

4.3 System topology comparison

Some proposed LCC circuits, such as [6] and [25], perform CC and CV operations for different load levels requiring a frequency control module. Contrary to this, the proposed topology can realize CC and CV charging with ZPA condition at a single frequency level. In practice, varying frequency

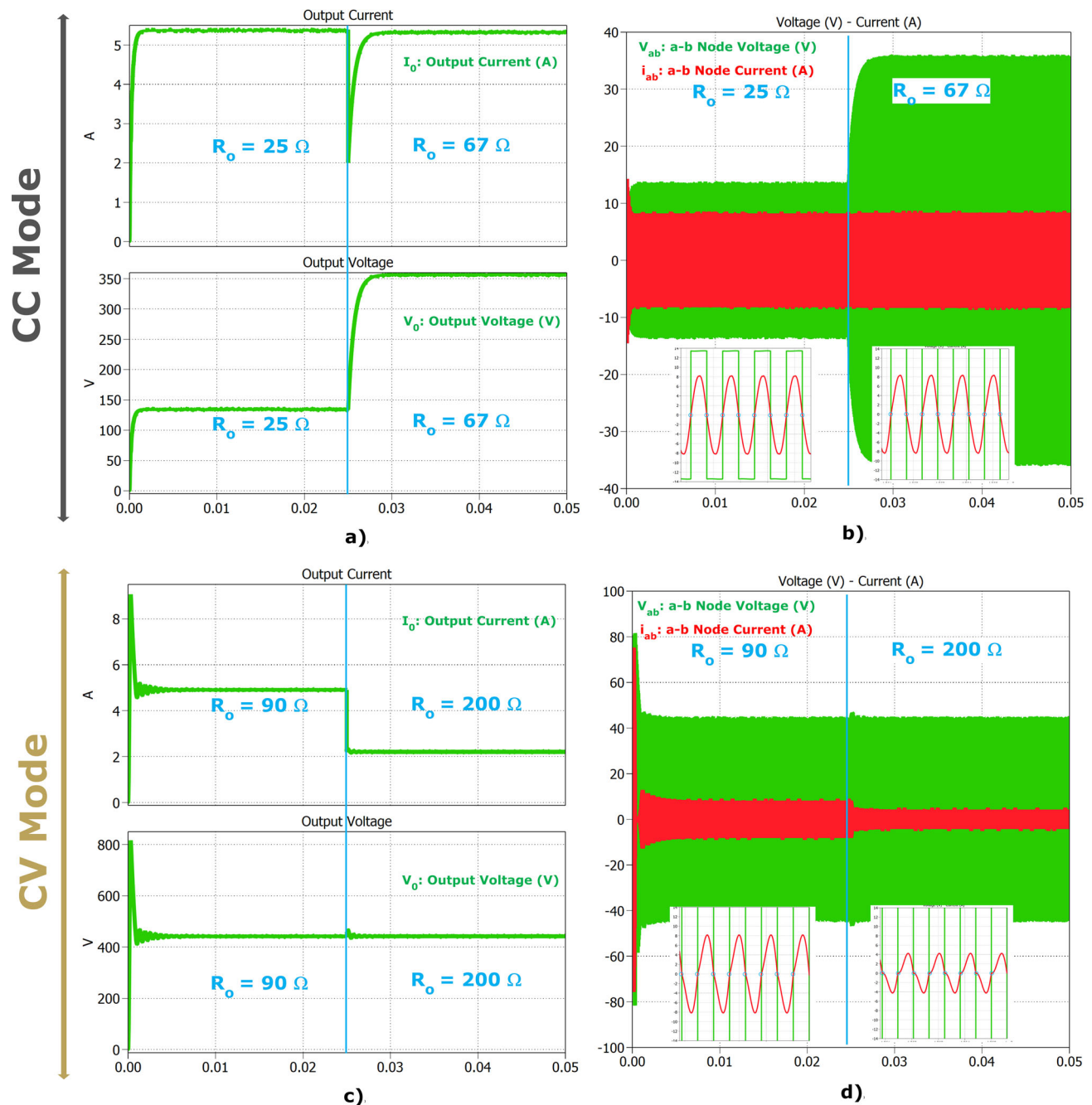


Fig. 19 The output current and voltage waveforms of the LCC circuit for $k = 0.4$ coupling factor, **a** output voltage and current waveforms in CC mode, **b** input current and voltage waveforms in CC mode, **c** output

voltage and current waveforms in CV mode, **d** input current and voltage waveforms in CV mode

according to the charging mode is not necessary. Therefore, a switching module is not required to achieve the CC and CV charging modes. In addition, according to the mathematical analysis and simulation results of the proposed topology, it has been verified that it can operate in CC and CV mode with ZPA at 85 kHz resonance frequency for different load conditions.

Switching between CC and CV charging modes can be implemented by simply controlling only one ACS at the same resonant frequency. As a result, the control circuit is easier and more feasible to implement as it requires single ACS control with simple control logic between the charging modes. Also, the proposed topology is less complex compared to other fixed frequency controlled and coupling

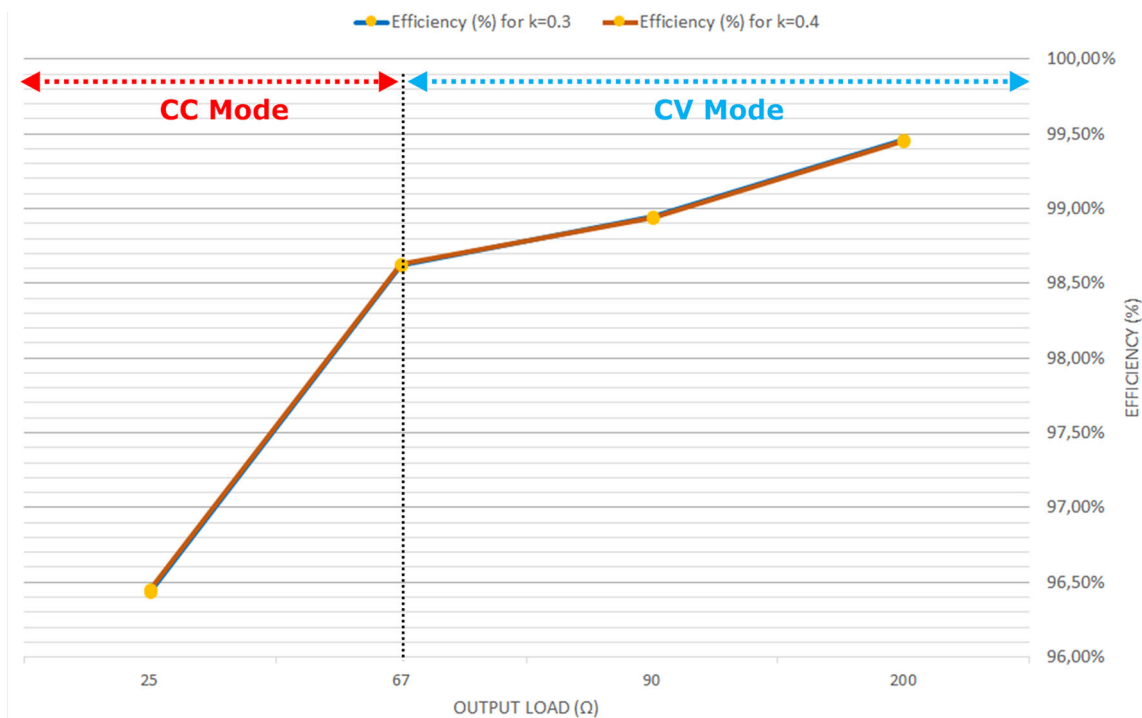


Fig. 20 Overall system efficiency for $k = 0.3$ and $k = 0.4$ coupling factors under the CC and CV charging modes

coefficient tuned resonant circuits due to its reduced number of components. In the proposed topology, using an extra capacitor on the transmitter side is not required to perform the CC and CV modes compared to the other studies. Moreover, the proposed topology includes fewer capacitors to achieve ZPA condition in both charging modes at a single resonant frequency. Hence, this provides the topology extending the lifespan of the circuit and making it less bulky due to the use of a reduced number of capacitors. Additionally, a comparison table among the proposed compensation topologies and discussed circuitries in the literature is demonstrated in Table 3.

Firstly, compared to the four main topologies such as SS, SP, PS and PP, the proposed topology is capable of performing CC and CV charge modes simultaneously with ZPA condition, but contains more components and increased circuit control complexity. Secondly, compared to the double-sided LCC topology demonstrated in [5] and [18], the proposed topology includes fewer components on the secondary side. Besides, the proposed system performs each charging mode without needing to change any mutual inductance value or resonant switching frequencies contrary to [5] and [18], simplifying the system's controlling process. The maximum efficiencies for the proposed topologies in [5] and [18] are 97.7 and 96.1%, respectively. The simulated efficiency of the proposed circuit is slightly better than the topologies studied in [5] and [18]. Third, the LCC-S topology presented in [6] requires dual resonant frequency control to realize

CC and CV output under ZPA condition, and the measured efficiency is 97.3% in [6]. This means different resonant frequency control for each charging mode, further complicating the control of the switches on the HV inverter side of the circuit. According to the study in [6], the proposed circuit requires the use of an additional tunable inductor and an ACS on the primary side of the circuit as a disadvantage. However, the proposed topology is slightly higher compared to [6]. Fourthly, the proposed design includes fewer capacitors according to the modified LCC-S circuitries presented in [24, 25] and [26]. In [24], the proposed topology uses a single switch, but it requires switching frequency tuning to perform CC/CV charging modes. Thus, it causes increased control complexity by adjusting the resonant frequency and encounters EMI problems. Additionally, the efficiency of the proposed system in [24] is 87%. In [25], the designed topology includes an additional capacitor and an ACS for each side of the circuit compared to the simple LCC-S circuit and the efficiency is measured as 89.28%. Moreover, two-sided-ACS control is required to provide stable CC and CV output, which causes sophisticated controlling and harms the WPT system's robustness. Also, the topology shown in [26] contains two additional ACSs and a single capacitor and inductor components on the secondary side, converting LCC-S to double-sided LCC. Moreover, the measured efficiency is 91% in [26]. Although these modified LCC-S circuitries are capable of performing CC and CV charging modes regardless of the battery load at a single switching frequency, they

Table 3 Comparison review between the proposed study and other related topologies

Topology type	Four main topologies				Double-sided LCC		LCC-S	Modified LCC-S			This Study
	SS	SP	PS	PP	[5]	[18]	[6]	[24]	[25]	[26]	
CC mode with ZPA	Yes	No	Not applicable	Yes	Yes	Yes	Yes	Yes	Yes	Yes	Yes
CV mode with ZPA	No	Yes	Yes	Not applicable	Yes	Yes	Yes	Yes	Yes	Yes	Yes
Varying Resonant Frequency	No	No	No	No	No	Yes	Yes	Yes	No	No	No
Tuning Mutual Inductance	No	No	No	No	Yes	No	No	No	No	No	No
Component Count	Low	Low	Low	Low	High	High	Medium	Medium	Very high	Very high	Medium
Control Complexity	Low	Low	Low	Low	High	Medium	Medium	High	High	High	Medium
Rated Power	–	–	–	–	8 kW	6.6 kW	3.5 kW	0.2 kW	2.5 kW	1.1 kW	2.4 kW
Measured Efficiency	–	–	–	–	97.1%	96.1%	97.3%	87%	89.28%	91%	98.66%

comprise more capacitors according to our proposed topology, which makes the circuits bulkier and complicated and shortens their lifetime. Compared to the studies in [24, 25] and [26], the simulated system performance of this study is enhanced, and the efficiency level is improved.

Although the use of a variable inductor in the proposed hybrid topology may introduce some challenges in terms of increased size and complexity compared to alternative approaches, it is important to note that these considerations must be weighed against the unique benefits it offers. The proposed topology achieves the load-independent ZPA condition, which enables efficient and seamless transitions between CC and CV charging modes at a single resonant frequency using a single AC switch. This simplifies control and operation, enhancing the overall charging efficiency and prolonging the battery lifespan. In addition, the reduced number of capacitors required by the proposed topology results in cost savings and enhanced reliability. Furthermore, the tunable inductor offers flexibility in system design and optimization, allowing for the adjustment of performance parameters. These benefits, along with the fixed operating frequency and the simplicity of a single switch, contribute to the development of IPT systems for efficient and dependable battery charging. Therefore, despite the potential size and complexity considerations, the proposed hybrid topology

offers notable advantages that justify its simple operation, increased reliability and further efficiency.

5 Conclusion

For wireless battery charging applications, load-independent CC and CV outputs at a single resonant frequency are possible by concentrating on the LCC-S compensation topologies. Hence, this study proposes a novel SS and LCC-S hybrid topology based on a tunable inductor and single ACS for inductive charging system to be used for inductive power transfer applications. By combining the SS and LCC-S topologies, the charging modes can be switched through a single ACS and a tunable inductor located on the primary side of the circuit. Therefore, the control complexity of the circuit can be reduced, and it makes the proposed circuit simpler. An additional benefit of the study is that CC and CV charging with ZPA condition can be provided at a fixed resonant frequency. Hence, this feature increases the reliability of the system.

In this paper, a 2.4 kW simulation prototype was built and analyzed extensively to validate the proposed circuit. The design techniques, and the mathematical analysis have been studied in detail. Furthermore, the simulation results of

the output current–voltage levels have been verified for various battery equivalent resistances. As a result, the desired charging current value of 6 A and the desired charging voltage value of 400 V were effectively achieved regardless of the battery charge level in CC and CV modes, respectively. The simulated efficiency of the maximum system power is measured as 98.66%. Hence, the simulation experiments approved the high stability of the proposed topology and its feasibility.

Author Contributions EK contributed to the study design, performing analysis, interpretation, and manuscript writing—editing. SB contributed to the study design, interpretation, supervision and manuscript editing.

Funding This study did not receive any funding.

Data availability This study did not use any data or materials that are publicly available.

Declarations

Conflict of interest The authors declare no competing interests.

Ethical Approval This study did not involve human or animal subjects, and thus, no ethical approval was required.

References

- Hwang S-H, Chen Y, Zhang H, Lee K-Y, Kim D-H (2020) Reconfigurable hybrid resonant topology for constant current/voltage wireless power transfer of electric vehicles. *Electronics* 9(8):1323. <https://doi.org/10.3390/ELECTRONICS9081323>
- Y Shou, B Luo, S Xiong, G Zhu, J Lu, J V Wang (2019) “Efficiency Analysis in IPT System Based on LCC Compensation Network,” *ICPE 2019 - ECCE Asia-10th International Conference on Power Electronics-ECCE Asia*, pp. 2258–2263, 2019, doi: <https://doi.org/10.23919/ICPE2019-ECCEASIA42246.2019.8796952>.
- Ali N, Liu Z, Armghan H, Ahmad I, Hou Y (2021) LCC-S-based integral terminal sliding mode controller for a hybrid energy storage system using a wireless power system. *Energies* 14(6):1693. <https://doi.org/10.3390/EN14061693>
- M Gholipour, S Farhangi, M Saradarzadeh, E Asadi (2021) “Implementation of Burp Pulse Charging in Inductive Power Transfer Systems with LCC-Series Compensating Topology for Electric Vehicle Charger Application,” *2021 12th Power Electronics, Drive Systems, and Technologies Conference, PEDSTC 2021*. doi: <https://doi.org/10.1109/PEDSTC52094.2021.9405885>.
- Li S, Li W, Deng J, Nguyen TD, Mi CC (2015) A double-sided LCC compensation network and its tuning method for wireless power transfer. *IEEE Trans Veh Technol* 64(6):2261–2273. <https://doi.org/10.1109/TVT.2014.2347006>
- Wang W, Deng J, Chen D, Wang Z, Wang S (2021) A novel design method of LCC-S compensated inductive power transfer system combining constant current and constant voltage mode via frequency switching. *IEEE Access*. <https://doi.org/10.1109/ACCESS.2021.3105103>
- Zhou S, Chris Mi C (2016) Multi-paralleled LCC reactive power compensation networks and their tuning method for electric vehicle dynamic wireless charging. *IEEE Trans Ind Electron* 63(10):6546–6556. <https://doi.org/10.1109/TIE.2015.2512236>
- Hannan MA, Hoque MM, Hussain A, Yusof Y, Ker PJ (2018) State-of-the-art and energy management system of lithium-ion batteries in electric vehicle applications: issues and recommendations. *IEEE Access* 6:19362–19378. <https://doi.org/10.1109/ACCESS.2018.2817655>
- Rehman M, Nallagownden P, Baharudin Z (2020) Design of a new hybrid topology of WPT system to achieve load-independent constant-current and constant-voltage output. *Symmetry* 12(9):1453. <https://doi.org/10.3390/SYM12091453>
- J Lu, G Zhu, W Li, B Li (2019) “Load-Independent ZPA Conditions in Both Constant Current and Constant Voltage Modes of LCC-Series Compensated IPT System,” *2018 IEEE Wireless Power Transfer Conference, WPTC 2018*, Feb. 2019, doi: <https://doi.org/10.1109/WPTC.2018.8639453>.
- Yan Z, Zhang Y, Song B, Zhang K, Kan T, Mi C (2019) “An LCC-P compensated wireless power transfer system with a constant current output and reduced receiver size. *Energies* 12(1):172. <https://doi.org/10.3390/EN12010172>
- Deng J, Li W, Li S, Mi C (2014) “Magnetic integration of LCC compensated resonant converter for inductive power transfer applications.” *2014 IEEE Energy Conversion Congress and Exposition ECCE 2014*:660–667. <https://doi.org/10.1109/ECCE.2014.6953458>
- Li S, Mi CC (2015) Wireless power transfer for electric vehicle applications. *IEEE J Emerg Sel Top Power Electron* 3(1):4–17. <https://doi.org/10.1109/JESTPE.2014.2319453>
- Vu VB, Phan VT, Dahidah M, Pickert V (2019) Multiple output inductive charger for electric vehicles. *IEEE Trans Power Electron* 34(8):7350–7368. <https://doi.org/10.1109/TPEL.2018.2882945>
- Zhang W, Mi CC (2016) Compensation topologies of high-power wireless power transfer systems. *IEEE Trans Veh Technol* 65(6):4768–4778. <https://doi.org/10.1109/TVT.2015.2454292>
- Sen Wang C, Stielau OH, Covic GA (2005) Design considerations for a contactless electric vehicle battery charger. *IEEE Trans Ind Electron* 52(5):1308–13145
- Qu X, Han H, Wong SC, Tse CK, Chen W (2015) Hybrid IPT topologies with constant current or constant voltage output for battery charging applications. *IEEE Trans Power Electron* 30(11):6329–6337. <https://doi.org/10.1109/TPEL.2015.2396471>
- Vu VB, Tran DH, Choi W (2018) Implementation of the constant current and constant voltage charge of inductive power transfer systems with the double-sided LCC compensation topology for electric vehicle battery charge applications. *IEEE Trans Power Electron* 33(9):7398–7410. <https://doi.org/10.1109/TPEL.2017.2766605>
- Thrimawithana DJ, Madawala UK (2013) A generalized steady-state model for bidirectional ipt systems. *IEEE Trans Power Electron* 28(10):4681–4689. <https://doi.org/10.1109/TPEL.2012.2237416>
- F. Lu, H. Hofmann, J. Deng, and C. Mi, “Output power and efficiency sensitivity to circuit parameter variations in double-sided LCC-compensated wireless power transfer system,” *Conference Proceedings - IEEE Applied Power Electronics Conference and Exposition - APEC*, vol. 2015-May, no. May, pp. 597–601, May 2015, doi: <https://doi.org/10.1109/APEC.2015.7104410>.
- Y Zhang, Y Guo, L Wang, Q Bo (2020) “Design of dual-side LCC compensation networks considering rectifier equivalent inductance for wireless power transfer system,” *2020 IEEE PELS Workshop on Emerging Technologies: Wireless Power Transfer, WoW 2020*, pp. 210–213. <https://doi.org/10.1109/WOW47795.2020.9291321>.
- Fu N, Deng J, Wang Z, Wang W, Wang S (2022) A hybrid mode control strategy for LCC-LCC-compensated WPT system with wide ZVS operation. *IEEE Trans Power Electron* 37(2):2449–2460. <https://doi.org/10.1109/TPEL.2021.3108637>
- Farajizadeh F, Vilathgamuwa DM, Jayathurathnage P, Ledwich G (2022) Estimation of the transferred power in LCC compensated

- wireless power transmitters with the use of PWM-synchronized sampling technique. *IEEE Trans Transport Electri* 8(1):710–722. <https://doi.org/10.1109/TTE.2021.3098643>
24. Zhang H, Chen Y, Park SJ, Kim DH (2019) A hybrid compensation topology with single switch for battery charging of inductive power transfer systems. *IEEE Access* 7:171095–171104. <https://doi.org/10.1109/ACCESS.2019.2955805>
 25. Chen Y, Zhang H, Park SJ, Kim DH (2019) A switching hybrid LCC-S compensation topology for constant current/voltage EV wireless charging. *IEEE Access* 7:133924–133935. <https://doi.org/10.1109/ACCESS.2019.2941652>
 26. Li G, Kim DH (2021) A wireless power transfer charger with hybrid compensation topology for constant current/voltage onboard charging. *Appl Sci* 11(16):7569. <https://doi.org/10.3390/APP11167569>
 27. UD Kavimandan VP Galigekere O Onar, M Mohammad, B Ozpineci, SM Mahajan (2021) “The sensitivity analysis of coil misalignment for a 200-kW dynamic wireless power transfer system with an LCC-S and LCC-P compensation,”2021 IEEE Transportation Electrification Conference and Expo, ITEC 2021, pp. 1–8. <https://doi.org/10.1109/ITEC51675.2021.9490035>.
 28. Chen Y, Zhang H, Park SJ, Kim DH (2019) A Comparative Study of S-S and LCCL-S Compensation Topologies in Inductive Power Transfer Systems for Electric Vehicles. *Energies* 12(10):1913. <https://doi.org/10.3390/EN12101913>
 29. Zhu Y, Wu H, Li F, Zhu Y, Pei Y, Liu W (2022) A comparative analysis of S-S and LCCL-S compensation for wireless power transfer with a wide range load variation. *Electronics*. <https://doi.org/10.3390/ELECTRONICS11030420>
 30. Zhao Q, Wang A, Liu J, Wang X (2019) The load estimation and power tracking integrated control strategy for dual-sides controlled LCC compensated wireless charging system. *IEEE Access* 7:75749–75761. <https://doi.org/10.1109/ACCESS.2019.2922329>
 31. D Medini, S Ben-Yaakov (1994) “A current-controlled variable-inductor for high frequency resonant power circuits,”*Conference Proceedings - IEEE Applied Power Electronics Conference and Exposition-APEC*, 1:219–225. <https://doi.org/10.1109/APEC.1994.316396>.

Publisher’s Note Springer Nature remains neutral with regard to jurisdictional claims in published maps and institutional affiliations.

Springer Nature or its licensor (e.g. a society or other partner) holds exclusive rights to this article under a publishing agreement with the author(s) or other rightsholder(s); author self-archiving of the accepted manuscript version of this article is solely governed by the terms of such publishing agreement and applicable law.